JACS
JOURNAL OF THE AMERICAN CHEMICAL SOCIETY

Article

pubs.acs.org/JACS

Columnar Liquid-Crystalline Metallomacrocycles

Shin-ichiro Kawano, Yukari Ishida, and Kentaro Tanaka*

Department of Chemistry, Graduate School of Science, Nagoya University, Furo-cho, Chikusa-ku, Nagoya 464-8602, Japan

Web-Enhanced Feature Supporting Information

ABSTRACT: We report synthesis of novel macrocyclic molecules and their metal complexes as well as their thermotropic columnar liquid-crystalline behavior. The macrocyclic ligands were prepared size-selectively based on dynamic covalent chemistry. X-ray study of a model macrocycle with short alkyl chains revealed that they were discrete and highly symmetric, with an inner vacant cavity of 9 Å diameter enclosed by a 56π planar ring composed of four bis(salicylidene)-*o*-phenylenediamine (salphen) moieties alternating with four carbazoles. Ni^{2+} and Cu^{2+} ions were incorporated into the four salphen ligands and formed square-planar metal complexes inside the macrocycles. From the structural and thermal analyses via X-ray diffraction measurements, differential scanning calorimetry, and polarized optical-microscopic observations, it was revealed that the macrocyclic ligand and its metal complexes self-assembled into columnar liquid-crystalline phases depending on the temperature and displayed a highly fluid character over a wide range of temperatures. The peripheral alkyl chains were influential in controlling the temperature range and flowability of the liquid-crystalline phases, and the range of the liquid-crystalline temperature of the metallo-macrocycles was significantly higher than those of the metal-free macrocycles. To the best of our knowledge, these are the first examples of thermotropic columnar liquid crystals of macrocyclic metal complexes with a large hollow area.

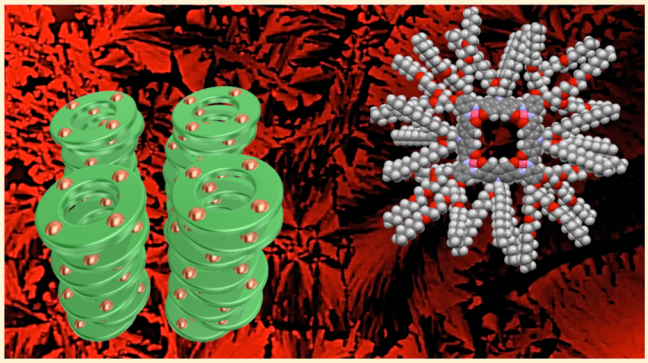

INTRODUCTION

Designer molecular nanospaces are promising systems for promoting multiple chemical processes such as specific recognition, storage, the construction of arrays, transportation, and the reactions of confined molecules.[1−5] Recently, many well-defined molecular nanospaces in crystalline materials have been reported. Some examples of such systems include the so-called metal−organic frameworks (MOFs),[4a] porous coordination polymers (PCPs),[4b] and covalent organic frameworks (COFs).[5] In contrast, only a few examples of nanospaces in fluid materials can be found in the literature. Nanochannels in columnar liquid crystals made from macrocyclic compounds could be candidates for soft molecular nanospaces that have flowable properties and the ability to undergo phase transitions (Figure 1).[6−8] Even if the continuous length of the nanochannel is quite short because of slippage in the stacking of the macrocycles, the cavities of the macrocycles themselves could behave as nanospaces that could incorporate guest molecules in the liquid crystal. However, it is generally difficult to synthesize a large macrocyclic molecule with a low phase-transition temperature. In addition, it is challenging to organize the macrocyclic molecules into homogeneously ordered columnar liquid-crystalline domains over a wide area. The difficulties depend on two principal factors. The first is the difficulty in the syntheses of large macrocyclic compounds with adequate nanospace to incorporate guest molecules. This restricts any enhancement in the flexibility of the molecular design. The second is that such large molecules usually have high phase-transition temperatures to liquid crystal and to isotropic liquids. In some cases, these temperatures are higher than the decomposition temperature of the macrocyclic molecule. For thermotropic liquid crystals, slow cooling from the isotropic phase is highly effective in obtaining homogeneously ordered liquid-crystalline phases. Generally, in the case of discotic columnar liquid crystals, peripheral alkyl chains surrounding a planar mesogen are key to lowering the phase-transition temperatures.[9]

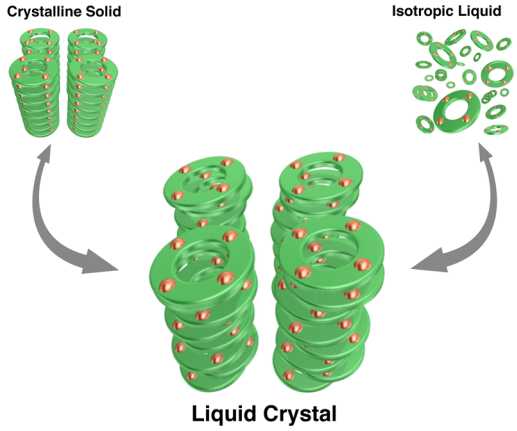

Figure 1. Columnar liquid-crystalline metallo-macrocycle.

Received: October 15, 2014
Published: February 6, 2015

DOI: 10.1021/ja510585u
J. Am. Chem. Soc. 2015, 137, 2295−2302

Scheme 1. Synthesis of the Macrocyclic Ligands via Dynamic Covalent-Bond Formation and a Schematic Illustration of the Macrocycles

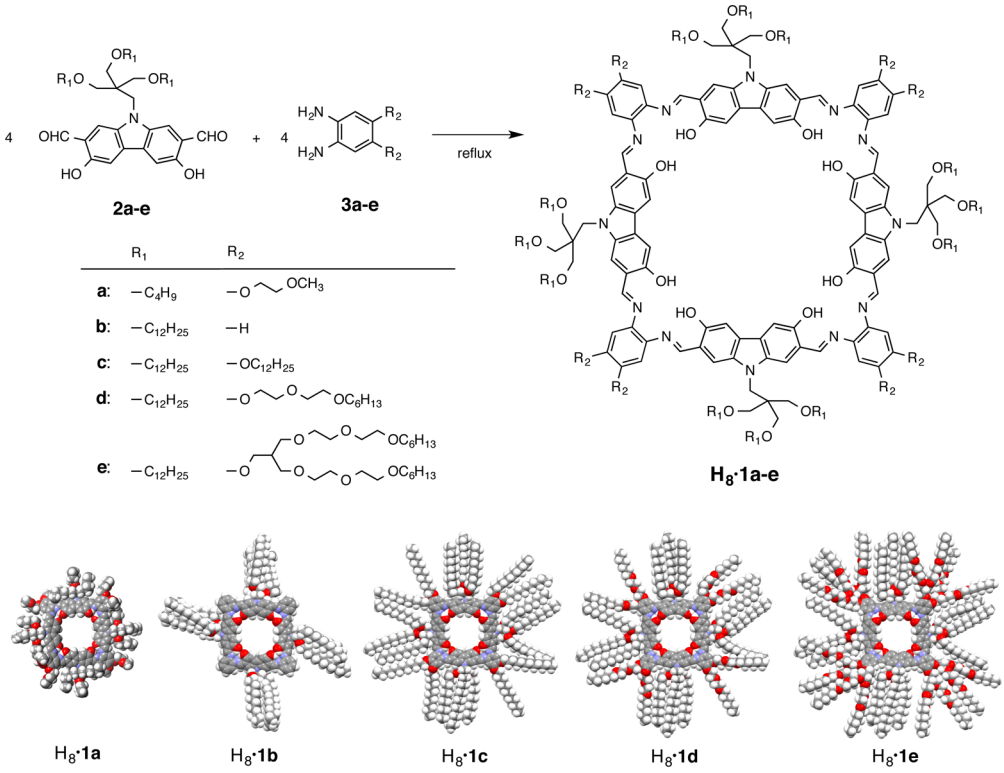

Although thermotropic macrocyclic columnar liquid crystals have been prepared through elegant coupling reactions in pioneering studies,[6,7] the extension of synthetic strategies and the diversification of structures and properties are still required to achieve the functionalization of the fluid nanospaces. In general, the synthetic yields of shape-persistent large macrocyclic compounds are relatively low. Careful design of the molecule and its usually multistep synthetic route, as well as purification of the desired product from similar byproducts, is required. In contrast, thermodynamically stable, unambiguous, and discrete products are afforded through self-assembly processes with reversible bond formation through coordination chemistry[10] or dynamic covalent chemistry.[11] In particular, the efficient synthetic strategies applied in the reversible formation and exchange processes of imines are known to afford large planar macrocycles.[12,13] *N*,*N*′-Bis(salicylidene)ethylenediamine (salen) and *N*,*N*′-bis(salicylidene)-*o*-phenylenediamine (salphen) moieties have been widely studied as a key unit of the large macrocycles, which are prepared through dynamic covalent-bond-formation processes between precursors, arenes with two carboxaldehyde moieties, and ethylenediamines or *o*-phenylenediamines. For the formation of discrete macrocyclic molecules, choosing carboxaldehyde moieties with appropriate relative geometries would yield a compatible polygon.

Salen and salphen have been used frequently as $[N_2O_2]$ planar metal ligands for various transition-metal ions, and the resulting metal complexes have been widely utilized as a central component in supramolecular, redox, magnetic, photophysical, and catalytic systems.[14] Therefore, the incorporation of the metal complexes inside the liquid-crystalline macrocycles would pave the way for the functionalization of the nanospaces. In addition, a variety of functions, depending on the kind of metal ions, could be imparted. Herein, we report the construction of a macrocyclic columnar liquid crystal for the development of well-defined molecular nanospaces in flowable media and the functionalization of the interior of the cavities by the incorporation of metal complexes (Figure 1).

RESULTS AND DISCUSSION

Syntheses and Structural Characterization of Macrocyclic Ligands and Metallo-Macrocycles. The first step in the construction of the macrocyclic columnar liquid crystal is the synthesis of a discrete and size-regulated macrocyclic compound composed of a planar macrocyclic mesogen and flexible alkyl chains. We designed imine-based macrocycles, H_8·**1a**−**e**, consisting of alternately linked carbazole and salphen moieties, as the base for the construction of a macrocyclic columnar liquid crystal. The alkyl chains surrounding the macrocyclic mesogen would effectively afford sufficient flexibility to allow liquid crystal formation.

The macrocycle H_8·**1e** was synthesized by a 4:4 condensation reaction between a carbazole with two carboxaldehydes at the 2- and 7-positions, **2e**, and *o*-phenylenediamine **3e** through an imine-based cyclization reaction in ethanol (Scheme 1). Although the reaction could have potentially yielded a mixture of different macrocycles and acyclic products, the ^{1}H NMR spectrum of the reaction mixture indicated the formation of a single main product with trace amounts of byproducts (Figure S1). After purification by gel permeation chromatography, the matrix-assisted laser desorption ionization time-of-flight (MALDI-TOF) mass spectrum of the main product showed a prominent single signal corresponding to the 4:4 macrocycle H_8·**1e** at *m*/*z* 7391.9 ($[M + H]^+$) (Figure 2a), indicating the selectivity of the reaction. The ^{1}H NMR spectrum of H_8·**1e** in $CDCl_3$ showed one set of proton signals for the carbazole and *o*-phenylenediamine units, with a new singlet imine signal at

DOI: 10.1021/ja510585u
J. Am. Chem. Soc. 2015, 137, 2295−2302

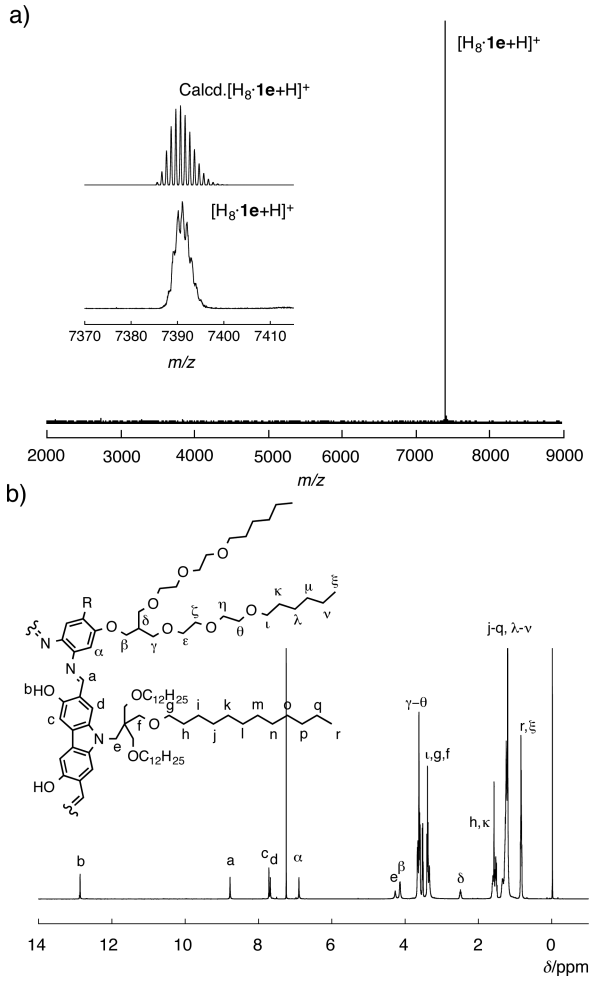

Figure 2. (a) MALDI-TOF mass spectrum of H_8·**1e** (matrix: dithranol) and (b) ^{1}H NMR (400 MHz) of H_8·**1e** in $CDCl_3$ at 293 K. The signals labeled with a ξ are assigned to the resonance of a quarter of the macrocycle.

8.78 ppm. This result suggested the presence of 4-fold rotational symmetry for the macrocycle, reflecting the right-angled geometries of the salphens bridged by the carbazoles (Figure 2b). H_8·**1a–d** macrocycles were obtained via a similar synthesis approach with similar cyclization efficiencies (see Supporting Information). H_8·**1a** is a model macrocycle with short alkyl chains for X-ray crystallography studies. H_8·**1b** has only 12 alkyl chains, whereas H_8·**1c** has 20 alkyl chains. The 20 alkyl chains of H_8·**1d** includes ether units that weaken the packing interactions between the alkyl chains. The H_8·**1e** macrocycle consists of a planar core and 28 peripheral alkyl chains including flexible ether-type alkyl chains on the phenylenediamine units. The inner and outer diameters of the mesogen were estimated to be 9 and 23–31 Å, respectively, from an X-ray single crystal analysis of the model macrocycle H_8·**1a** (Figure 3). All of the phenyl rings of the salphen moieties were arranged on the outer circumference of the mesogen. In addition, the OH substituents of the salphens were directed inward and bound with the imino N atoms via hydrogen bonding with an average O···N distance of 2.62(1) Å. In the series of macrocycles, the hydrogen bonds seem to be effective in restricting the rotation of the carbazole moieties, and as a consequence, all the alkyl chains of the macrocycle would radiate in all directions without occupying the interior of their own inner space. Although the π-plane of each carbazole adopted

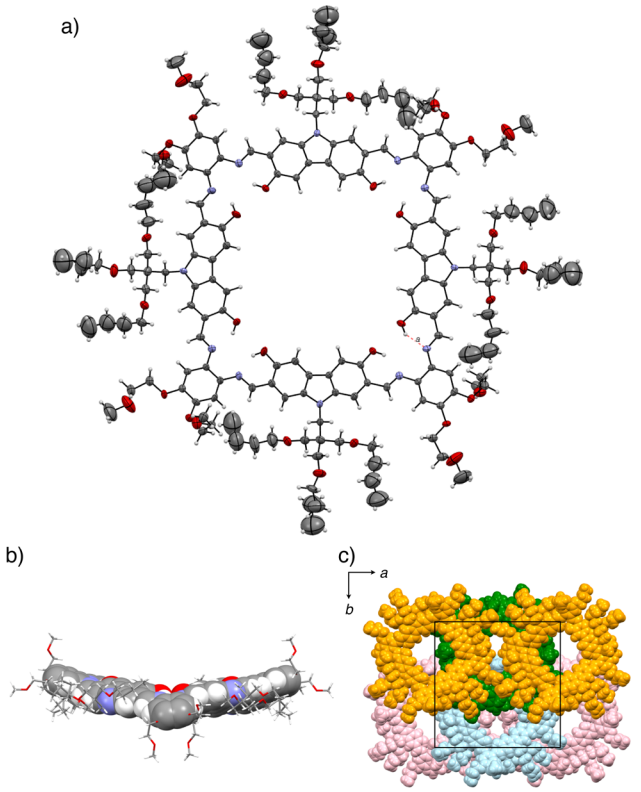

Figure 3. Crystal structure of H_8·**1a**. (a) ORTEP diagram with the thermal ellipsoids at a 50% probability level, (b) side view of the macrocycle, and (c) molecular packing of H_8·**1a** from a view along the *c*-axis.

a twisted conformation with relatively small angles of 23°–26° in the crystal of H_8·**1a**, which are comparable to the angles found by the 3:3 macrocycles of Nabeshima[12a] and MacLachlan,[13d] the 4-fold-rotational symmetry structure of the mesogen structure in a solution is obvious from the relatively simple NMR spectra of the macrocycles (vide supra). The structural feature of the mesogenic macrocycle is suited for columnar stacking in the liquid-crystalline phases. Moreover, the planar conjugated 56π–π system of the mesogenic unit was identified by the characteristic absorption peak at 438 nm via UV–vis spectroscopy due to the extended π-system of the macrocycles (Figure 4).

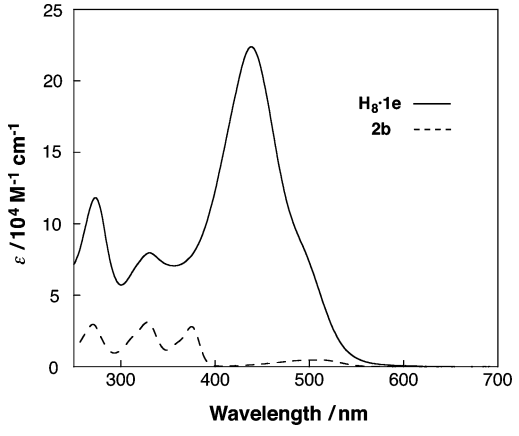

Figure 4. Absorption spectra of macrocycle H_8·**1e** and the carbazole precursor **2b**. The spectra were measured in [H_8·**1e**] = 3.0 × 10^{-6} M and [**2b**] = 12 × 10^{-6} M, respectively, in $CHCl_3$.

DOI: 10.1021/ja510585u
J. Am. Chem. Soc. 2015, 137, 2295–2302

Scheme 2. Synthesis of Metallo-Macrocycles M_4·1d, M_4·1e, Where M Is Ni or Cu

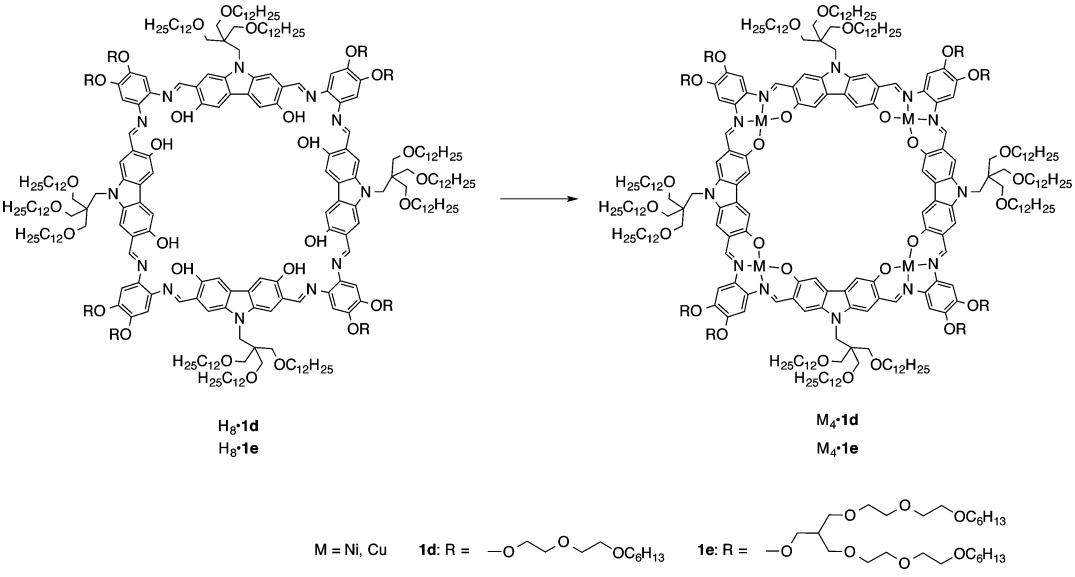

Tetranuclear Ni(II) and Cu(II) complexes of the H_8·**1d** and H_8·**1e** macrocycles were synthesized next (Scheme 2). Owing to the deprotonation of phenolic protons from each salphen ligand during the metal complexation, the metallo-macrocycles are completely uncharged. Tetranuclear Ni(II) complexes (Ni_4·**1d** and Ni_4·**1e**) showed sharp narrow ^{1}H NMR signals, indicating the formation of diamagnetic square-planar complexes without axial ligands (Figure S4). The 4-fold symmetry of the ^{1}H NMR spectra of the metallo-macrocycles also indicated a highly symmetric mesogen structure without distortion through metal complexation.

Liquid-Crystalline Properties of the Macrocyclic Ligands. The thermal phase behaviors of macrocycles H_8·**1b-e** were analyzed by thermogravimetric analysis (Figures S5 and S6), differential scanning calorimetry (DSC, Figures 5 and S7), and

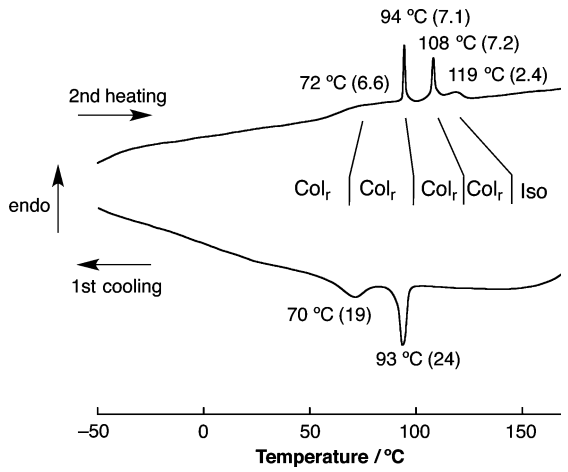

Figure 5. DSC trace of H_8·**1e** for the first cooling and the second heating cycles with a scanning rate of 10 °C/min. Phase notation is as follows: Col_r, columnar rectangular phase; Iso, isotropic melt. Transition enthalpies (kJ/mol) are given in parentheses.

polarized optical microscopy (POM, Figures 6 and S9). In the DSC measurement of H_8·**1e** from −60 to 180 °C, four distinct endothermic peaks were observed at 72.4, 94.4, 108, and 119 °C

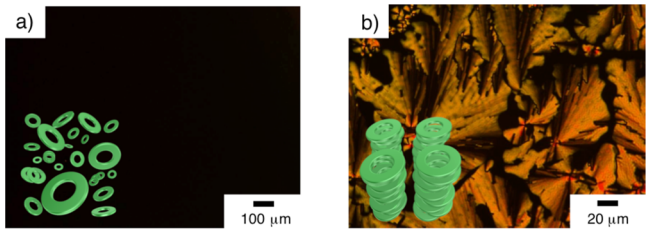

Figure 6. POMs of H_8·**1e**. (a) an isotropic liquid (Iso) at 130 °C and (b) a rectangular columnar phase (Col_r) at 105 °C on cooling from the isotropic melt.

(Figure 5). The transition recorded by DSC at 119 °C corresponded to the clearing point in the POM observation, whereas H_8·**1b** and H_8·**1c** decomposed before their melting points were reached. Upon cooling H_8·**1e** from the isotropic temperature (melting temperature), a columnar liquid-crystalline phase with a fan-shaped texture was observed from just below the melting temperature (Figure 6). The texture of the sample wedged between the slide and the cover glass plates deformed to a sticky fluid upon soft tapping at the top of the cover glass plate. (See Movie 1, a Web-enhanced object, which represents the real-time observation of that at 110 °C.) Around each phase-transition temperature of the liquid-crystalline phases, there were no significant changes in the birefringent texture. Even at room temperature, the liquid-crystalline material showed high fluid and the fan-shaped texture. Therefore, the H_8·**1e** macrocycle formed very fluid liquid-crystalline phases in a wide temperature range including at temperatures below the room temperature.

The molecular orientations of the H_8·**1e** macrocycles in the liquid-crystalline phases were revealed by X-ray diffraction (XRD) of the macrocycle encapsulated in a capillary and by a grazing incidence wide-angle X-ray scattering (GIWAXS) study of a thin film of the macrocycle on a glass plate. In the XRD study at 112 °C (Figure 7a), four diffraction peaks were found at small angles. All the diffraction peaks observed were in complete agreement with a rectangular arrangement of a columnar stacked macrocycle. The dimensions of the unit cell were calculated as a = 45.3 Å and b = 35.7 Å, respectively, resulting in an area that closely agreed with the molecular area of the planar macrocyclic plane and alkyl chain substituents which

DOI: 10.1021/ja510585u
J. Am. Chem. Soc. 2015, 137, 2295−2302

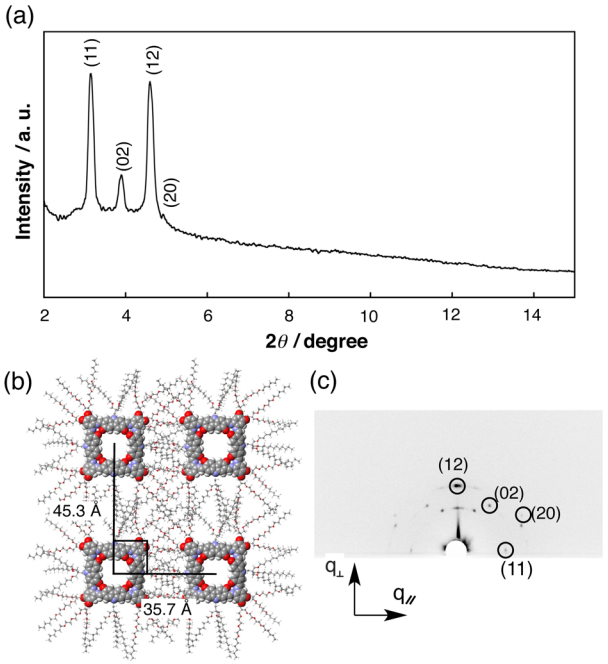

Figure 7. (a) XRD pattern of H_8·**1e** at 112 °C on heating. Values in parentheses are Miller indices, (b) a postulated columnar packing of H_8·**1e** in an orthorhombic lattice deduced from the GIWAXS data (see Table S3 for the lattice parameters), and (c) GIWAXS pattern of H_8·**1e** placed on a glass substrate at 112 °C.

radiate outward (Figure 7b), whose molecular model is supported by solid state NMR measurements. The 2D hetronuclear correlation (HETCOR) spectrum of H_8·**1e** in the liquid-crystalline phase revealed that the aliphatic alkyl chains were segregated from the rigid macrocyclic mesogen and there was no proximity of the side chains to the inside of the macroccyle (Figure S25).[7d] The GIWAXS study revealed several discrete Bragg reflections that demonstrated a distinct parallel orientation of the column to the surface of a glass substrate.[15] The distance and direction of the anisotropic spots conformed to the indexes obtained from the powder XRD measurements (Figure 7c). XRD studies of H_8·**1e** at 105 °C, 85 °C, and 26 °C revealed that the molecular orientations consisted of a rectangular columnar phase at all the temperatures. There are no significant textural changes in the POM observations (Figure S22) and no orientation changes of the columns on the substrate except for small changes in the intercolumnar distances in the GIWAXS measurements (Figure S21) among the consecutive multiple rectangular columnar phases. This type of phase transition between same packing geometries in discotic columnar liquid crystals is not unusual, and the phenomena were concluded as the results of a conformational change of the peripheral side chains or slight inter- and intracolumnar packing rearrangement.[16] In the rectangular columnar phases of the macrocycle H_8·**1e**, the 2D lattice areas calculated from the lattice parameters were smaller at the higher temperature. Although the stacking distances between the macrocycles along the columnar axes were not observed in the XRD measurements, the phase transitions would be expected to cause changes in the stacking angles of the macrocycle.

The liquid-crystalline property of H_8·**1d** with fewer alkyl chains was also investigated. The H_8·**1d** macrocycle formed three different liquid-crystalline phases (disordered nematic columnar (N_c), oblique columnar (Col_{ob}), and rectangular columnar (Col_r) phases) according to the temperature and displayed a highly fluid character between 75 and 208 °C (Figure 8). Upon cooling of H_8·**1d** from the isotropic temperature, a disordered nematic columnar liquid-crystalline phase with a schlieren texture was observed from just below the melting temperature up to 200 °C (Figure 9b). Although a phase transition was not detected by DSC, the POM image substantially changed to a mosaic texture at 200 °C representing a columnar phase, and

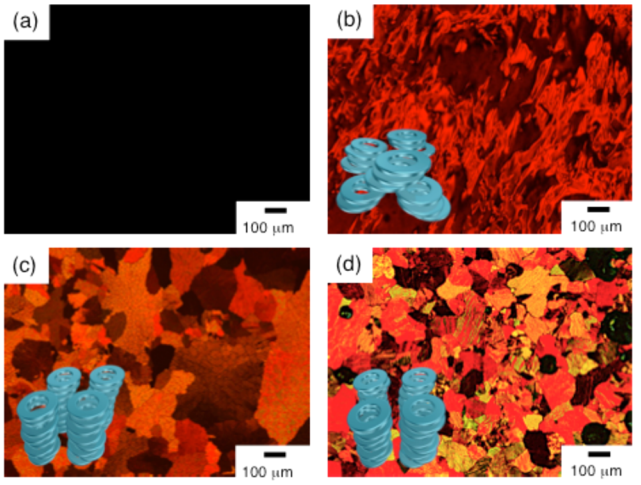

Figure 9. POMs of H_8·**1d** at various temperatures, upon cooling from the isotropic melt (a) an isotropic liquid (Iso) at 220 °C, (b) a columnar nematic phase (N_c) at 203 °C, (c) an oblique columnar phase (Col_{ob}) at 180 °C, and (d) a rectangular columnar phase (Col_r) at 140 °C.

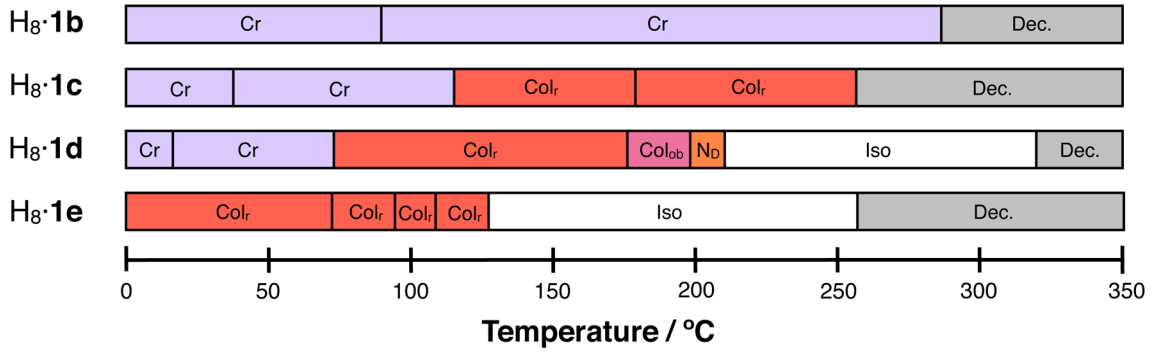

Figure 8. Phase diagrams of the macrocycles H_8·**1b–e** traced during the second heating cycle in DSC with a heating rate of 10 °C/min. Phase notations: Cr, crystal; Col_r, rectangular columnar liquid-crystalline phase; Col_{ob}, oblique columnar liquid-crystalline phase; N_c, columnar nematic liquid-crystalline phase; Iso, isotropic liquid.

DOI: 10.1021/ja510585u
J. Am. Chem. Soc. 2015, 137, 2295–2302

the birefringent domains were about a few hundred mm in size (Figure 9c). This phase obviously displayed an oblique columnar packing in both the XRD and GIWAXS measurements (Figures S12 and S13 and Table S2). Between the phase transitions at 178 and 75 °C, a slight change in the birefringent mosaic texture was observed from the oblique columnar phase at higher temperatures, and the XRD study at 140 °C demonstrated a rectangular columnar phase (Figures S12 and S13). This macrocycle was crystallized below 75 °C.

The ability to transition between phases and fluidities of the material was significantly influenced by the number and the chemical structure of the side chains surrounding the mesogen. The H_8·**1b** macrocycle, bearing fewer alkyl chains, only adopted the crystalline state, whereas liquid-crystalline H_8·**1c** with simple hydrocarbon chains decomposed before the melting temperature to the isotropic liquid was reached. Hence, the flexible alkyl chains of H_8·**1d** and H_8·**1e** are suitable for forming liquid crystals of the macrocyclic mesogen and the denser alkyl chains of H_8·**1e** lowered the liquid crystallization temperature effectively.

Liquid-Crystalline Behaviors of the Metallo-Macrocycles. Metallo-macrocycles Ni_4·**1d** and Cu_4·**1d** showed fluidic character with orientational order above the phase-transition temperature from crystalline states at 117.6 and 111.4 °C, respectively, which are close to the phase-transition temperature between crystal and liquid crystal of H_8·**1d**. However, these metallo-macrocycles do not have melting temperatures below the decomposition temperatures. Consequently, large birefringent domains were not observed in the POM images even after long annealing, although the XRD measurements revealed transitions of some columnar liquid-crystalline phases upon heating.

In contrast, the melting temperature of Ni_4·**1e** is at 340 °C, which is below its decomposition temperature. By slow cooling through the melting temperature, a birefringent fan-shaped texture appeared in the POM image (Figure 10). Ni_4·**1e** showed liquid-crystalline properties from 340 and 110 °C and became solidified via the phase transition at 110 °C (Figure 11). The XRD measurement clearly demonstrated the formation of rectangular columnar phases, which are similar to that of H_8·**1e** (Figure S17).

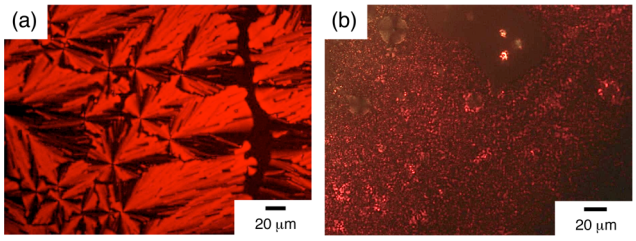

Figure 10. POMs of (a) Ni_4·**1e** and (b) Cu_4·**1e** at 112 °C.

However, Ni_4·**1e** formed a liquid crystal phase in the higher temperature region, which is probably caused by the improvement in the flatness and a lowering of the degree of flexibility of the macrocycle through the formation of square-planar metal complexes. In the case of the tetranuclear copper complex, although Cu_4·**1e** decomposed at 220 °C before the liquid crystal-to-isotropic liquid transition temperature, crystal-to-liquid crystal transition was observed in the similar temperature region as the tetranickel complex. To our best knowledge, these are the first examples of columnar liquid crystals of macrocyclic metal complexes. The salphen ligand can coordinate to a variety of transition-metal ions, and the complexes have been widely utilized as a component of supramolecular, redox, magnetic, photophysical, and catalytic materials. The inside of the macrocycle could be functionalized as a unique nanospace in the liquid-crystalline material by metal complexation.

■ CONCLUSIONS

In conclusion, we selectively and efficiently synthesized the macrocycles H_8·**1a-e** consisting of a planar 56π ring as the mesogen and peripheral alkyl chains via the self-assembly process utilizing aldimine-formation reaction. X-ray crystal studies of H_8·**1a** revealed that the macrocycle has an inner circular nanospace with a diameter of 9 Å. In spite of the large mesogen size, the H_8·**1d** and H_8·**1e** macrocycles have phase-transition temperatures to isotropic liquids below their decomposition temperatures, showed enantiotropic liquid-crystalline properties with multistep phase transitions, and formed large uniform liquid-crystalline domains. The peripheral alkyl chains were influential in controlling the temperature range and flowability of the liquid-crystalline phases. The four salphens in the macrocyclic ring have the potential to bind various metal ions. Four liquid-crystalline tetranuclear macrocyclic complexes were synthesized. Among them, Ni_4·**1e** in particular, formed large liquid-crystalline domains, which had a fan-shaped texture upon slow cooling from the isotropic temperature, in which the macrocyclic metal complexes were stacked in a rectangular columnar fashion similar to the metal-free H_8·**1e** macrocycle. The range of the liquid-crystalline temperature of the metallo-macrocycle was significantly higher than that of the metal-free macrocycle, probably because of stiffer and higher planarity of the metallo-macrocycle. The temperature range could be controlled by varying the number and the chemical structure of the peripheral alkyl chains.

These interesting macrocyclic arrays offer a variety of opportunities for development. The functions and the properties of metal ions introduced into the mesogen and the inner cavities of the ring provide sufficiently large nanospaces that interact with guest molecules. We are currently investigating the expansion of the molecular design of the macrocycles,

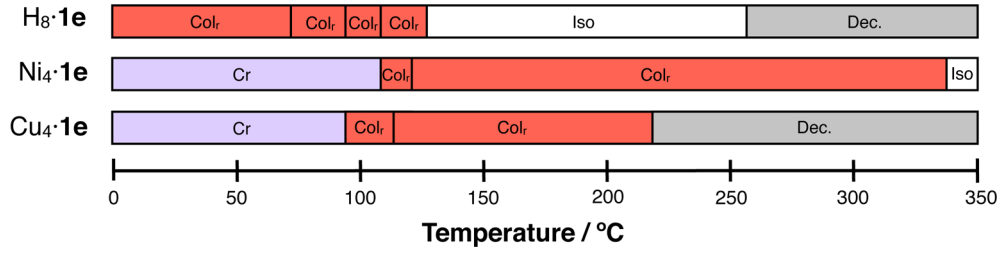

Figure 11. Phase diagrams of the metallo-macrocycles Ni_4·**1e** and Cu_4·**1e** traced the second heating cycle on DSC with heating rate of 10 °C/min. Phase notations: C_r, crystal; Col_r, rectangular columnar liquid-crystalline phase; Iso, isotropic liquid.

DOI: 10.1021/ja510585u
J. Am. Chem. Soc. 2015, 137, 2295−2302

coordination with a variety of metals, and the inclusion of guest molecules into the nanospaces.

EXPERIMENTAL SECTION

Materials and Methods. Synthetic procedures were carried out under dry nitrogen atmosphere, unless otherwise specified. All reagents and solvents were purchased at the highest commercial quality available and used without further purification, unless otherwise stated. ^{1}H and ^{13}C NMR spectra were recorded on a JEOL JNM-ECS400 (400 MHz for ^{1}H; 100 MHz for ^{13}C) spectrometer at a constant temperature of 298 K. Tetramethylsilane (TMS) was used as an internal reference for ^{1}H and ^{13}C NMR measurements in $CDCl_3$. MALDI-TOF-MS was performed with an ultraflex III, Bruker Daltonics, and α-CHCA was used as the matrix. Elemental analyses were performed on a Yanaco MT-6 analyzer. Silica gel column chromatographies and thin-layer (TLC) chromatography were performed using Merck silica gel 60 and Merck silica gel 60 (F254) TLC plates, respectively. GPC was performed using a JAI LC-9204 equipped with JAIGEL columns.

*Macrocycle H_8·**1a**.* Carbazole **2a** (0.17 g, 0.31 mmol) and **3a** (81 mg, 0.31 mmol) were stirred in dry EtOH (23 mL) at reflux for 48 h, then a red precipitate was obtained. The crude product was filtered and purified by GPC (JAIGEL 2.5H-2.5H, $CHCl_3$) and followed by recrystallization from ethanol to obtain a red solid as a target compound H_8·**1a** (95 mg, 31 μmol, 40%) ^{1}H NMR (400 MHz, $CDCl_3$, TMS): δ 12.8 (s, 8H), 8.78 (s, 8H), 7.72 (s, 8H), 7.67 (s, 8H), 6.96 (s, 8H), 4.31−4.26 (m, 24H), 3.85−3.82 (m, 16H), 3.48 (s, 24H), 3.41 (t, J = 6.4 Hz, 24H), 3.36 (s, 24H), 1.63−1.54 (m, 24H), 1.45−1.41 (m, 24H), 0.92 (t, J = 7.2 Hz, 36H). ^{13}C NMR (100 MHz, $CDCl_3$/TMS): δ = 161.2, 154.3, 149.0, 138.4, 136.9, 126.4, 119.6, 112.7, 107.6, 104.5, 71.1, 71.0, 69.3, 59.2, 47.4, 43.5, 32.0, 29.7, 19.6, 14.0. MS (MALDI-TOF, Matrix: dithranol, RP-Mode) m/z 3048.8: calcd for $C_{172}H_{236}N_{12}O_{36}H$ $[M + H]^+$; found: 3048.0.

*Macrocycle H_8·**1b**.* H_8·**1b** was synthesized by the similar procedure described for the synthesis of the macrocycle H_8·**1a** (17 mg, 4.4 μmol, 38%). ^{1}H NMR (400 MHz, $CDCl_3$, TMS): δ 12.7 (s, 8H), 8.84 (s, 8H), 7.73 (s, 16H), 7.26 (s, 3H), 4.30 (s, 2H), 4.06 (m, 3H), 3.42−3.39 (m, 6H), 3.36 (s, 5H), 1.64 (m, 8H), 1.25−1.21 (m, 54H), 0.88−0.82 (m, 9H). ^{13}C NMR (100 MHz, $CDCl_3$/TMS): δ = 163.0, 154.5, 143.5, 127.7, 126.7, 119.5, 118.5, 113.0, 107.8, 71.4, 69.1, 47.4, 31.9, 30.0, 29.7, 29.3, 26.4, 22.7, 14.1. MS (MALDI-TOF, Matrix: α-CHCA, RP-Mode) m/z 3802.8: calcd for $C_{244}H_{380}N_{12}O_{20}H$ $[M + H]^+$; found; m/z 3801.6. Anal. calcd for $C_{244}H_{380}N_{12}O_{20}$: C, 77.09; H, 10.07; N 4.42. Found: C, 77.28; H, 10.15; N, 4.32.

*Macrocycle H_8·**1c**.* H_8·**1c** was synthesized by the similar procedure described for the synthesis of the macrocycle H_8·**1a** (37 mg, 27 μmol, 49%). ^{1}H NMR (400 MHz, $CDCl_3$, TMS): δ 12.9 (s, 8H), 8.80 (s, 8H), 7.72−7.70 (m, 16H), 6.89 (s, 16H), 4.28 (s, 8H), 4.09−4.08 (m, 16H), 3.44−3.42 (m, 24H), 3.36−3.35 (m, 24H), 1.89−1.86 (m, 16H), 1.67−1.64 (m, 16H), 1.56−1.21 (m, 368H), 0.90−0.84 (m, 60H). ^{13}C NMR (100 MHz, $CDCl_3$, TMS): δ = 160.6 154.3 149.3, 138.4, 126.4, 119.6, 112.5, 107.7, 103.2, 71.2, 69.7, 69.0, 47.4, 32.0, 30.0, 29.8, 29.7, 29.5, 29.4, 26.5, 26.2, 22.7, 14.1. MS (MALDI-TOF, α-CHCA, RP-Mode): calcd for $C_{340}H_{572}N_{12}O_{28}H$ $[M + H]^+$, m/z 5277.4, found; m/z 5277.4 Anal. calcd for $C_{340}H_{572}N_{12}O_{28}$: C, 77.40; H, 10.93; N 3.19. Found: C, 77.01; H, 10.95; N, 2.94.

*Macrocycle H_8·**1d**.* H_8·**1d** was synthesized by the similar procedure described for the synthesis of the macrocycle H_8·**1a** (0.18 g, 34 μmol, 48%). ^{1}H NMR (400 MHz, $CDCl_3$, TMS): δ 12.8 (s, 8H), 8.79 (s, 8H), 7.73 (s, 8H), 7.69 (s, 8H), 6.96 (s, 8H), 4.29−4.27 (m, 24H), 3.95−3.93 (m, 16H), 3.78−3.76 (m, 16H), 3.64−3.61 (m, 16H), 3.45 (t, J = 6.8 Hz, 16H), 3.41 (t, J = 6.3 Hz, 24H), 3.30 (s, 24H), 1.65−1.54 (m, 40H), 1.36−1.23 (m, 288H), 0.88−0.84 (m, 60H). ^{13}C NMR (100 MHz, $CDCl_3$/TMS): δ = 161.2, 154.4, 149.0, 138.4, 137.0, 126.5, 119.6, 112.6, 107.8, 104.6, 71.7, 71.3, 71.0, 70.2, 69.8, 69.5, 69.1, 47.4, 31.9, 31.7, 29.8, 29.7, 29.6, 29.4, 26.4, 25.8, 22.7, 22.6, 14.1, 14.0. MS (MALDI-TOF, Matrix: α-CHCA, RP-Mode) m/z 5308.9: calcd for $C_{324}H_{540}N_{12}O_{44}H$ $[M + H]^+$, found: 5310.0. Anal. calcd for $C_{324}H_{540}N_{12}O_{44}$: C, 73.32; H, 10.25; N 3.17. Found: C, 73.50; H, 10.19; N, 3.19.

*Macrocycle H_8·**1e**.* H_8·**1e** was synthesized by the similar procedure described for the synthesis of the macrocycle H_8·**1e** (30 mg, 4.1 μmol, 22%). ^{1}H NMR (400 MHz, $CDCl_3$, TMS): δ 12.9 (s, 8H), 8.79 (s, 8H), 7.73 (s, 8H), 7.70 (s, 8H), 6.91 (s, 8H), 7.16 (s, 8H), 4.27 (s, 8H), 4.16 (d, J = 3.6 Hz, 16H), 3.68−3.60 (m, 128H), 3.55−3.53 (m, 32H), 3.43−3.36 (m, 80H), 2.52−2.49 (m, 8H), 1.62−1.53 (m, 56H), 1.40−1.22 (m, 336H), 0.87−0.83 (m, 84H). ^{13}C NMR (100 MHz, $CDCl_3$/TMS): δ = 160.9, 154.4, 149.1, 138.3, 136.3, 126.4, 119.6, 112.5, 107.8, 103.2, 71.6, 71.2, 70.7, 70.5, 69.3, 69.1, 67.4, 47.4, 40.2, 31.9, 31.7, 29.8, 29.7, 29.6, 25.8, 22.7, 22.6, 14.1. MS (MALDI-TOF, Matrix: (dithranol, RP-Mode) m/z 7391.9: calcd for $C_{436}H_{764}N_{12}O_{76}H$ $[M + H]^+$, found: 7391.2. Anal. calcd for $C_{436}H_{764}N_{12}O_{76}$: C, 70.85; H, 10.42; N 2.27. Found: C, 71.05; H, 10.67; N, 2.25.

*Ni Complex Ni_4·**1d**.* H_8·**1d** (27 mg, 5.1 mmol) and $Ni(OAc)_2{\cdot}4H_2O$ (5.8 mg, 23 mmol) were dissolved in $CHCl_3$ (3.8 mL) and EtOH (3.8 mL). The reaction mixture was stirred at 90 °C for 5h. The reaction mixture was filtrated, and a precipitate was washed with $CHCl_3$. The filtrate was evaporated to obtain a crude product. The crude product was purified by GPC (JAIGEL 3H-2.5H, $CHCl_3$) to obtain a reddish violet solid (25 mg, 4.6 mmol, 88%). ^{1}H NMR (400 MHz, $CDCl_3$, TMS): δ 8.18 (s, 8H), 7.88 (s, 8H), 7.36 (s, 8H), 7.24 (s, including $CHCl_3$ 8H), 4.30−4.15 (m, 16H), 4.06 (s, 8H) 3.95−3.85 (m, 16H), 3.82−3.68 (m, 16H), 3.66−3.54 (m, 16H), 3.53−3.32 (m, 64H), 1.72−1.66 (m, 16H), 1.62−1.52 (m, 24H), 1.51−1.36 (m, 24H), 1.38−1.10 (m, 256H), 0.92−0.78 (m, 60H). MS (MALDI-TOF, Matrix: dithranol, RP-Mode) m/z 5535.6: calcd for $C_{324}H_{532}N_{12}Ni_4O_{44}H$ $[M + H]^+$, found: 5535.7. Anal. calcd for $C_{324}H_{532}N_{12}Ni_4O_{44}$: C, 70.31; H, 9.69; N 3.04. Found: C, 70.37; H, 9.93; N, 3.19.

*Cu Complex Cu_4·**1d**.* H_8·**1d** (14 mg, 2.6 mmol) was dissolved in chloroform (1.9 mL) and ethanol (1.9 mL). $Cu(OAc)_2$ (2.1 mg, 11 mmol) was added to the solution. The reaction mixture was refluxed for 17.5 h. The solution was filtered through, and the GPC (JAIGEL, 20 f, 3H-2.5H) was used for the purification. The resultant residue was further purified by recrystallization from ethanol twice to afford the target compound as a purple solid (11 mg, 2.0 mmol 75%). MS (MALDI-TOF, Matrix: dithranol, RP-Mode) m/z 5555.0: calcd for $C_{324}H_{532}Cu_4N_{12}O_{44}H$ $[M + H]^+$, found: 5554.8. Anal. calcd for $C_{324}H_{532}Cu_4N_{12}O_{44}$: C, 70.07; H, 9.65; N 3.03. Found: C, 70.27; H, 9.72; N 2.83.

*Ni Complex Ni_4·**1e**.* Ni_4·**1e** was synthesized by the similar procedure described for the synthesis of the macrocycle Ni_4·**1d** (25 mg, 3.2 μmol, 79%). ^{1}H NMR (400 MHz, $CDCl_3$, TMS): δ 8.16 (s, 8H), 7.91 (s, 8H), 7.36 (s, 8H), 7.16 (s, 8H), 4.14 (s, 16H), 4.05 (s, 8H), 3.65−3.61 (m, 128H), 3.56−3.54 (m, 32H), 3.45−3.40 (m, 80H), 2.53−2.47 (m, 8H), 1.66−1.51 (m, 56H), 1.40−1.22 (m, 312H), 0.87−0.83 (m, 84H). ^{13}C NMR (100 MHz, $CDCl_3$/TMS): δ = 160.0, 153.6, 152.2, 150.8, 149.1, 138.6, 136.5, 131.9, 120.6126.4, 119.6, 112.5, 107.8, 103.2, 71.6, 71.2, 70.7, 70.5, 69.3, 69.1, 67.4, 47.4, 40.2, 31.9, 31.7, 29.8, 29.7, 29.6, 25.8, 22.7, 22.6, 14.1. MS (MALDI-TOF, Matrix: dithranol, RP-Mode) m/z 7618.6: calcd for $C_{436}H_{756}N_{12}Ni_4O_{76}H$ $[M + H]^+$, found: 7617.6. (ESI-TOF MS, NaI was added, positive) m/z 2562.1: calcd for $C_{436}H_{756}N_{12}Ni_4O_{76}$ ($[M + 3Na]^{3+}$), found: 2561.7, m/z 1927.3: calcd for $C_{436}H_{756}N_{12}Ni_4O_{76}$ ($[M + 4Na]^{4+}$), found: 1927.3, m/z 1546.5: calcd for $C_{436}H_{756}N_{12}Ni_4O_{76}$ ($[M + 5Na]^{5+}$), found: 1546.5. Anal. calcd for $C_{436}H_{756}N_{12}Ni_4O_{76}$: C, 68.90; H, 10.00; N 2.21. Found: C, 68.90; H, 10.16; N, 2.27.

*Cu Complex Cu_4·**1e**.* Cu_4·**1e** was synthesized by the similar procedure described for the synthesis of the macrocycle Cu_4·**1d** (18 mg, 2.4 μmol, 47%). MS (MALDI-TOF, Matrix: dithranol, RP-Mode) m/z 7638.0: calcd for $C_{436}H_{756}Cu_4N_{12}O_{76}H$ $[M + H]^+$, found: 7637.6. Anal. calcd for $C_{436}H_{756}Cu_4N_{12}O_{76}$: C, 68.57; H, 9.98; N 2.20. Found: C, 68.55; H, 10.14; N 2.25.

Structural and Thermal Measurements of the Macrocycles. DSC measurements were carried out under N_2 atmosphere with TA Instruments Q2000 DSC equipped with a RCS 90 cooling accessory, and the transition temperatures were determined from the second heating run at a rate of 10 °C/min using Universal Analysis 2000 software. TGA analysis was performed under N_2 atmosphere with TA Instruments TGAQ50 with the temperature raised from 30 to 600 °C at a rate of 10 °C/min. POM observations were performed with a

DOI: 10.1021/ja510585u
J. Am. Chem. Soc. 2015, 137, 2295−2302

OLYMPUS BX51 microscope with crossed polarizers, Linkam LTS 350 heating stage under N_2 atmosphere, and a OLYMPUS DP20 camera. XRD and GIWAXS analyses were measured using a Rigaku R-AXIS IV X-ray diffractometer (CuK_α) equipped with a temperature controlled heating stage and an imaging plate for collection of the diffracted patterns. GIWAXS analysis of the sample placed on the glass plate was measured with the temperature-controlled heating stage heated at the various temperatures. The incidence angle was set to ~0.4°. The diffracted radiation was recorded by imaging plate that has the sample-to-detector distance of 30 cm, with exposure time of 3 min. The absorption spectra were recorded with a Hitachi U-4100 spectrophotometer in $CHCl_3$ solutions at 20 ± 0.1 °C in 1.0 cm quartz cells.

■ ASSOCIATED CONTENT

Supporting Information

Experimental details, ^1H NMR spectra of H_8·**1e** before and after GPC purification, TGA, DSC, PXRD, GIWAXS analyses, and UV−vis absorption spectra of the macrocyclic ligands and macrocyclic metal complexes. This material is available free of charge via the Internet at http://pubs.acs.org.

Web-Enhanced Feature

A movie of the real-time observation of the liquid-crystalline phase of H_8·**1e** at 110 °C is available in the HTML version of the paper.

■ AUTHOR INFORMATION

Corresponding Author

*kentaro@chem.nagoya-u.ac.jp

Notes

The authors declare no competing financial interest.

■ ACKNOWLEDGMENTS

We thank Dr. Kinichi Oyama of the Chemical Instrumentation Faculty, Research Center for Materials Science, Nagoya University, for elemental analysis. We thank Dr. M. Hara, Mr. T. Hikage, Dr. S. Saito (Nagoya University), and Prof. S. Sasaki (Kyoto Institute of Technology) for their fruitful suggestions and technical assistance in the X-ray measurements. We also appreciate Institute of Transformative Bio-Molecules (WPI-ITbM, Nagoya University) for giving us permission to use their single crystal analyzer. We also thank Yuichi Shimoikeda (JEOL resonance Inc.) and Dr. Yutaka Maeda (Nagoya University) in the solid-state NMR measurements. This work was financially supported by Grant-in-Aids for Scientific Research on Innovative Areas "Coordination Programming" (area 2107, no. 21108012) and The Japan Securities Scholarship Foundation to K.T.

■ REFERENCES

(1) Steed, J. W.; Atwood, J. L. *Supramolecular Chemistry*, 2nd ed.; Wiley: West Sussex, U.K., 2009.

(2) (a) Gokel, G. W.; Carasel, I. A. *Chem. Soc. Rev.* **2007**, *36*, 378−389. (b) Matile, S.; Jentzsch, A. V.; Montenegro, J.; Fin, A. *Chem. Soc. Rev.* **2011**, *40*, 2453−2474.

(3) (a) Kitagawa, S.; Matsuda, R. *Coord. Chem. Rev.* **2007**, *251*, 2490−2509. (b) Li, J. R.; Kuppler, R. J.; Zhou, H. C. *Chem. Soc. Rev.* **2009**, *38*, 1477−1504.

(4) (a) Eddaoudi, M.; Moler, D. B.; Li, H.; Chen, B.; Reineke, T. M.; O'keeffe, M.; Yaghi, O. M. *Acc. Chem. Res.* **2001**, *34*, 319−330. (b) Kitagawa, S.; Kitaura, R.; Noro, S. *Angew. Chem., Int. Ed.* **2004**, *43*, 2334−2375.

(5) (a) Côté, A. P.; Benin, A. I.; Ockwig, N. W.; O'Keeffe, M.; Matzger, A. J.; Yaghi, O. M. *Science* **2005**, *310*, 1166−1170. (b) Furukawa, H.; Yaghi, O. M. *J. Am. Chem. Soc.* **2009**, *131*, 8875−8883. (c) Urive-Romo, F. J.; Hunt, J. R.; Furukawa, H.; Klöck, C.; O'Keeffe, M.; Yaghi, O. M. *J. Am. Chem. Soc.* **2009**, *131*, 4570−4571.

(6) (a) Zhang, J.; Moore, J. S. *J. Am. Chem. Soc.* **1994**, *116*, 2655−2656. (b) Mindyuk, O. Y.; Stetzer, M. R.; Heiney, P. A.; Nelson, J. C.; Moore, J. S. *Adv. Mater.* **1998**, *10*, 1363−1366.

(7) (a) Höger, S. *Chem.—Eur. J.* **2004**, *10*, 1320−1329. (b) Höger, S.; Enkelmann, V.; Bonrad, K.; Tschierske, C. *Angew. Chem., Int. Ed.* **2000**, *39*, 2268−2270. (c) Fischer, M.; Lieser, G.; Rapp, A.; Schnell, I.; Mamdouh, W.; Feyter, S. D.; Schryver, F. C. D.; Höger, S. *J. Am. Chem. Soc.* **2011**, *126*, 214−222. (d) Fritzsche, M.; Dudenko, A. B. D.; Baumeister, U.; Sebastiani, D.; Richardt, G.; Spiess, H. W.; Hansen, R.; Höger, S. *Angew. Chem., Int. Ed.* **2011**, *50*, 3030−3033.

(8) (a) Stepien, M.; Donnio, B.; Sessler, J. L. *Angew. Chem. Int. Ed.* **2007**, *46*, 1431−1435. (b) Sato, K.; Itoh, Y.; Aida, T. *J. Am. Chem. Soc.* **2011**, *133*, 13767−13769. (c) Norouzi-Arasi, H.; Pisula, W.; Mavrinskiy, A.; Feng, X.; Müllen, K. *Chem.—Asian J.* **2011**, *6*, 367−371.

(9) (a) Laschat, S.; Baro, A.; Steinke, N.; Giesselmann, F.; Hägele, C.; Scalia, G.; Judele, R.; Kapatsina, E.; Sauer, S.; Schreivogel, A.; Tosoni, M. *Angew. Chem., Int. Ed.* **2007**, *46*, 4832−4887. (b) Bushby, R. J.; Lozman, O. R. *Curr. Opin. Colloid Interface Sci.* **2002**, *7*, 343−354. (c) Kumar, S. *Chem. Soc. Rev.* **2006**, *35*, 83−109. (d) Wu, J.; Pisula, W.; Müllen, K. *Chem. Rev.* **2007**, *107*, 718−747.

(10) (a) Sun, E.-Y.; Yoshizawa, M.; Kusukawa, T.; Fujita, M. *Curr. Opin. Chem. Biol.* **2002**, *6*, 757−764. (b) Chakrabarty, R.; Mukherjee, P. S.; Stang, P. J. *Chem. Rev.* **2011**, *111*, 6810−6918.

(11) (a) Oh, K.; Jeong, K.-S.; Moore, J. S. *Nature* **2001**, *414*, 889−893. (b) Zhao, D.; Moore, J. S. *Macromolecules* **2003**, *36*, 2712−2720. (c) Jin, Y.; Yu, C.; Denman, R. J.; Zhang, W. *Chem. Soc. Rev.* **2013**, *42*, 6634−6654.

(12) (a) Akine, S.; Taniguchi, T.; Nabeshima, T. *Tetrahedron Lett.* **2001**, *42*, 8861−8864. (b) Akine, S.; Hashimoto, D.; Saiki, T.; Nabeshima, T. *Tetrahedron Lett.* **2004**, *45*, 4225−4227. (c) Akine, S.; Sunaga, S.; Taniguchi, T.; Miyazaki, H.; Nabeshima, T. *Iorg. Chem.* **2007**, *46*, 2959−2961. (d) Nabeshima, T. *Bull. Chem. Soc. Jpn.* **2010**, *83*, 969−991.

(13) (a) Gallant, A. J.; MacLachlan, M. J. *Angew. Chem., Int. Ed.* **2003**, *42*, 5307−5310. (b) Ma, C. T. L.; MacLachlan, M. J. *Angew. Chem., Int. Ed.* **2005**, *44*, 4178−4182. (c) Ma, C.; Abdolmaleki, A.; MacLachlan, M. J. *Org. Lett.* **2004**, *6*, 3841−3844. (d) Gallant, A. J.; Hui, J. K.-H.; Zahariev, F. E.; Wang, Y. A.; MacLachlan, M. J. *J. Org. Chem.* **2005**, *70*, 7936−7946. (e) MacLachlan, M. J. *Pure. Appl. Chem.* **2006**, *78*, 873−888. (f) Hui, J. K.-H.; MacLachlan, M. J. *Chem. Commun.* **2006**, 2480−2482. (g) Frischmann, P. D.; Jiang, J.; Hui, J. K.-H.; Grzybowski, J. J.; MacLachlan, M. J. *Org. Lett.* **2008**, *10*, 1255−1258. (h) Jiang, J.; MacLachlan, M. J. *Chem. Commun.* **2009**, 5695−5697. (i) Guieu, S.; Crane, A. K.; MacLachlan, M. J. *Chem. Commun.* **2011**, *47*, 1169−1171.

(14) (a) Whiteoak, C. J.; Salassa, G.; Kleij, A. W. *Chem. Soc. Rev.* **2012**, *41*, 622−631. (b) Kingsborough, R. P.; Swager, T. M. *Adv. Mater.* **1998**, *10*, 1100−1104. (c) Miyasaka, H.; Clérac, R.; Wernsdorfer, W.; Lecren, L.; Bonhomme, C.; Sugiura, K.-i.; Yamashita, M. *Angew. Chem., Int. Ed.* **2004**, *43*, 2801−2805. (d) Splan, K. E.; Massari, A. K. M.; Morris, G. A.; Sun, S.-S.; Reina, E.; Nguyen, S. T.; Hupp, J. T. *Eur. J. Iorg. Chem.* **2003**, 2348−2351. (e) Zhang, W.; Loebach, J. L.; Wilson, S. R.; Jacobsen, E. N. J. *Am. Chem. Soc.* **1990**, *112*, 2801−2803. (f) Katsuki, T. *Chem. Soc. Res.* **2004**, *33*, 437−444.

(15) (a) Pouzet, E.; Cupere, V. D.; Heintz, C.; Andreasen, J. W.; Breiby, D. W.; Nielsen, M. M.; Viville, P.; Lazzaroni, R.; Gbabode, G.; Geerts, Y. H. *J. Phys. Chem. C* **2009**, *113*, 14398−14406. (b) Grelet, E.; Dardel, S.; Bock, H.; Goldmann, M.; Lacaze, E.; Nallet, F. *Eur. Phys. J. E* **2010**, *31*, 343−349. (c) Hara, M.; Nagano, S.; Seki, T. *J. Am. Chem. Soc.* **2010**, *132*, 13654−13656.

(16) (a) Ito, S.; Ando, M.; Nomura, A.; Morita, N.; Kabuto, C.; Mukai, H.; Ohta, K.; Kawakami, J.; Yoshizawa, A.; Tajiri, A. *J. Org. Chem.* **2005**, *70*, 3939−3949. (b) Jiang, J.; Shen, Z.; Lu, J.; Fu, P.; Lin, Y.; Tang, H.; Gu, H.; Sun, J.; Xie, P.; Zhang, R. *Adv. Mater.* **2004**, *16*, 1534−1538. (c) Tanaka, S.; Sakurai, T.; Honsho, Y.; Saeki, A.; Seki, S.; Kato, K.; Tanaka, M.; Osuka, A.; Aida, T. *Chem.—Eur. J.* **2012**, *18*, 10554−10561. (d) Gearba, R. I.; Lehmann, M.; Levin, J.; Ivanov, D. A.; Koch, M. H. J.; Barberá, J.; Debije, M. G.; Piris, J.; Geerts, Y. H. *Adv. Mater.* **2003**, *15*, 1614−1618.

DOI: 10.1021/ja510585u
J. Am. Chem. Soc. 2015, 137, 2295−2302